J Electroceram (2007) 18:111–120
DOI 10.1007/s10832-007-9021-x

Oxygen reduction at thin dense $La_{0.52}Sr_{0.48}Co_{0.18}Fe_{0.82}O_{3-\delta}$ electrodes

Part II: Experimental assessment of the reaction kinetics

Michel Prestat · Anna Infortuna · Sybille Korrodi · Samuel Rey-Mermet · Paul Muralt · Ludwig J. Gauckler

Received: 29 August 2005 / Accepted: 13 December 2006 / Published online: 23 March 2007

Abstract The mechanism and kinetics of oxygen reduction at thin dense two-dimensional $La_{0.52}Sr_{0.48}Co_{0.18}Fe_{0.82}O_{3-\delta}$ (LSCF) electrodes have been investigated in air between 500 and 700 °C with electrochemical impedance spectroscopy and steady-state voltammetry. Dense and geometrically well-defined LSCF films with various thicknesses ranging between 16 and 766 nm have been prepared on cerium gadolinium oxide substrates by pulsed laser deposition and structured with photolithography. The current collection was ensured by a porous LSCF layer. A good agreement was found between the experimental data and the impedance of the reaction model calculated with state-space modelling for various electrode potentials and thicknesses. It was evidenced that oxygen adsorption, incorporation into the LSCF and bulk diffusion are rate-determining while charge transfer at the electrode/electrolyte interface remains at quasi-equilibrium. The 16 and 60 nm thin dense LSCF electrodes appear to be more active towards oxygen reduction than thicker layers and porous films at 600 and 700°C.

Keywords Oxygen reduction · Solid oxide fuel cells · Dense films · Impedance spectroscopy · Grain size

M. Prestat (✉) · A. Infortuna · S. Korrodi · L. J. Gauckler
ETH-Zurich, Institute for Nonmetallic Inorganic Materials,
Wolfgang-Pauli-Strasse 10, HCI G531,
Zurich 8093, Switzerland
e-mail: michel.prestat@mat.ethz.ch

S. Rey-Mermet · P. Muralt
Ceramics Laboratory, École Polytechnique
Fédérale de Lausanne (EPFL),
Lausanne 1015, Switzerland

1 Introduction

In a previous paper [1], a model for oxygen reduction at thin dense $La_{0.52}Sr_{0.48}Co_{0.18}Fe_{0.82}O_{3-\delta}$ (LSCF) perovskite electrodes at intermediate temperatures has been proposed. The corresponding faradaic impedance has been calculated with state-space modelling. The aim of the present work was to test the suggested reaction mechanism by comparing simulated and experimental data. The latter were obtained from a model interface that consisted of a polished gadolinium-doped ceria (CGO) on top of which a thin dense LSCF layer with well-controlled dimensions was prepared by pulsed lased deposition (PLD) and subsequently structured with photolithography. Geometrically well-defined electrodes that allow for the control of key parameters, such as the length of triple phase boundary (*tpb*) gas/electrode/electrolyte and the bulk diffusion length, become increasingly popular for experimental investigations of reaction mechanisms [2–6] in the field of SOFC. In this study the variation of the film thickness has been used to probe the influence of oxygen bulk diffusion on the overall reaction kinetics. The impedance and the steady-state polarization of oxygen reduction have been measured in air between 500 and 700 °C. A numerical optimisation process enabled to test the validity of the reaction model and to assess the rate constants. The electrochemical performance of the PLD films was also compared with the one of porous electrodes.

2 Reaction model and strategy

The model for oxygen reduction at LSCF electrodes accounts for bulk and surface reaction pathways. Yet the

surface pathway contribution can be ignored since simulations show it is negligible due to limited *tpb*-length [1]. In the Kröger–Vink notation, the bulk pathway is written as follows:

Adsorption:

$$O_{2(g)} + 2s \underset{K_{des}}{\overset{K_{ads}}{\rightleftarrows}} 2O_{ads} \tag{1}$$

Oxygen exchange (incorporation) between the adsorbate and the LSCF:

$$O_{ads} + V^{\cdot\cdot}_{O(mc)} + 2Co^{x}_{Co(mc)} \underset{K_{out}}{\overset{K_{in}}{\rightleftarrows}} O^{x}_{O(mc)} + 2C^{\cdot}_{Co(mc)} + s \tag{2}$$

$$O_{ads} + V^{\cdot\cdot}_{O(mc)} + 2Co^{'}_{Co(mc)} \underset{K_{out}}{\overset{K_{in}}{\rightleftarrows}} O^{x}_{o(mc)} + 2Co^{x}_{Co(mc)} + s \tag{3}$$

with s being in a non-occupied adsorption site at the surface of the LSCF.

Diffusion of oxygen vacancies:

$$V^{\cdot\cdot}_{O(mc)} \xrightarrow{D} V^{\cdot\cdot}_{O(mc)} \tag{4}$$

Oxygen exchange at the LSCF/CGO interface:

$$O^{x}_{O(mc)} + V^{\cdot\cdot}_{O(CGO)} \underset{K_{bb}}{\overset{K_{fb}}{\rightleftarrows}} V^{\cdot\cdot}_{O(mc)} + O^{x}_{O(CGO)} \tag{5}$$

All the rate constants of the model are independent of the potential E and the thickness d of the LSCF electrode, except K_{fb} and K_{bb} that are functions of E:

$$K_{fb} = k_{fb} e^{-2\alpha f E} \tag{6}$$

$$K_{bb} = k_{bb} e^{2(1-\alpha) f E} \tag{7}$$

with α being the charge transfer coefficient and f having the same meaning as in [1].

Additionally the defect chemistry of the LSCF film has been described by a random defect model [1, 7]. The cobalt and iron cations are believed to be distributed randomly on the B sites of the perovskite and are treated as "equal". The defect chemistry model includes a disproportionation reaction that is assumed to remain at quasi-equilibrium.

$$2Co^{x}_{Co} \underset{}{\overset{K_{\alpha}}{\rightleftarrows}} Co^{'}_{Co} + Co^{\cdot}_{Co} \tag{8}$$

Local electroneutrality as well as conservation of oxygen sites and B sites have been considered. The validity of the model was restricted to oxygen vacancy ratios lower than 25% (at which LSCF is completely reduced). The fixed parameters implemented in the state-space model are listed in Table 1.

The other parameters are not known accurately enough to be directly implemented in the model. They constitute the vector $\boldsymbol{p}=[\delta, N, K_{ads}, K_{des}, K_{out}, D, k_{fb}]$, N being the surface concentration of adsorption sites. In the following we denote Z_{sim} and Z_{exp} the simulated and experimental impedances. Both Z_{sim} and Z_{exp} are functions of the electrode potential, E, the thickness, d, of the dense LSCF layer (DL) as well as on the pulsation ω. Z_{sim} depends also on the vector $\boldsymbol{p}$ whose components have been adjusted in a numerical optimisation process (NOP) to describe at best the experimental impedance spectra.

$$Z_{sim} = Z_{sim}(E, d, \omega, \boldsymbol{p}) \tag{9}$$

$$Z_{exp} = Z_{exp}(E, d, \omega) \tag{10}$$

Z_{sim} is composed of the faradaic impedance $Z_F(\boldsymbol{p})$, the impedance Z_e that accounts for the ohmic drop in the electrolyte between the working and the reference electrodes and the double layer capacitance C_{DL} at the electrode/electrolyte interface (Fig. 1). R_e and C_{DL} are assumed to be independent of E, ω and $\boldsymbol{p}$. R_1 is the charge transfer resistance and Z_c is the concentration impedance.

Table 1 Fixed parameters and concentration of the key-species in LSCF at 500 and 600 °C in air under equilibrium.

	600 °C	500 °C	Remarks/references
M (g mol^{-3})	218.6	218.6	
ρ25 (g cm^{-3})	6.25	6.25	At 25 °C
ρ (g cm^{-3})	6.07	6.10	
[Sr] (mol L^{-1})	12.7	13.4	
[O] (mol L^{-1})	79.2	83.8	
[Co]+[Fe] (mol L^{-1})	26.4	27.9	
K_{α}	3.63 10^{-4}	5.72 10^{-5}	[7] Extrapolated values
α	0.5	0.5	

The density at room temperature has been linearly interpolated from the values obtained at various strontium contents [8–10]. The density ρ is calculated by taking into account the linear expansion between room temperature to the final temperature [10].

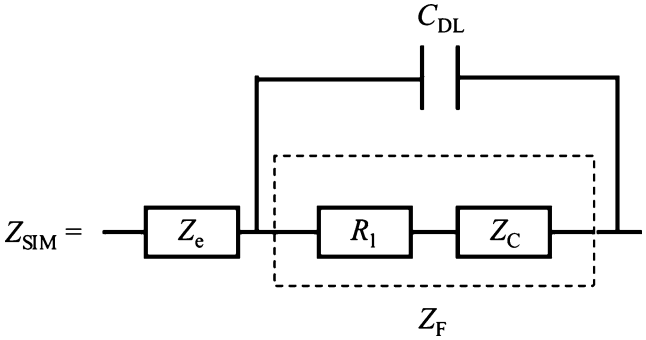

Fig. 1 Structure of the simulated impedance: Z_{sim} includes the faradaic impedance Z_F calculated with state-space modelling, the electrolyte impedance Z_e and the double layer capacitance C_{DL}

The polarisation resistance R_p is defined as

$$R_p = R_1 + Z_c(\omega \to 0) - Z_c(\omega \to \infty) \tag{11}$$

For the NOP, the following residual function h has been used

$$h(\boldsymbol{p}) = \frac{1}{a} \times \frac{1}{b}\sum_E \sum_d \sum_\omega \frac{\left|Z_{sim}(E,d,\omega,\boldsymbol{p}) - Z_{exp}(E,d,\omega)\right|^2}{\left|Z_{sim}(E,d,\omega,\boldsymbol{p})\right|\left|Z_{exp}(E,d,\omega)\right|} \tag{12}$$

where a is the number of experimental points per impedance plot and b the number of doublets (E, d) used for one numerical optimisation run. The function h tends towards 0 when Z_{sim} tends towards Z_{exp}.

Data taken from the literature enable to estimate the order of magnitudes of δ, K_{out} and D. The oxygen vacancy diffusivity D can be derived from the oxygen self diffusion coefficient D_O by using the relation:

$$C_V D = C_O D_O \tag{13}$$

where C_O and C_V are the concentrations of oxygen and oxygen vacancy at equilibrium respectively.

In the isotope exchange depth profile technique (IEDP) [11, 12], the surface exchange coefficient k is defined by

$$k = \frac{J_O}{C_O} \tag{14}$$

with J_O being the flux of oxygen crossing the gas/solid interface. Consequently, in our reaction model, the rate constant K_{out} can be related to k [1]:

$$k \approx K_{out} N (1 - x_{eq}) \left(\left[Co^x_{Co}\right]^2_{eq} + \left[Co^{\cdot}_{Co}\right]^2_{eq} \right) \tag{15}$$

with x_{eq}, $\left[Co^x_{Co}\right]_{eq}$ and $\left[Co^{\cdot}_{Co}\right]_{eq}$ having the same meaning as in [1].

The range of investigation of the ***p***-components is listed in Table 2. The numerical simulations were performed with the software packageMatlab® 6.5/Simulink® 6 (Mathworks Inc.) using the toolboxes "Control System" (version 5) and "Optimisation" (version 3).

3 Experimental

3.1 Preparation of CGO pellets

The electrolyte was prepared by pressing uniaxially and then isostatically (850 kN for 3 min) from commercially available $Ce_{0.9}Gd_{0.1}O_{1.95}$ powder (Rhodia, La Rochelle, France). The resulting pellets were heated up to 1400 °C with a rate of 3 °C min^{-1}, held at this temperature for 4 h and cooled down to room temperature at 5 °C min^{-1}. The density of the pellets was then evaluated using the Archimedes's method and reached 98% of the theoretical value. The CGO substrates have been polished with SiC paper.

3.2 Fabrication of thin LSCF films by PLD

The LSCF targets have been prepared from commercially available powder (Praxair Specialty Ceramics, USA) by uniaxial pressing and subsequent isostatic pressing (850 kN for 3 min). Then the LSCF pellets were sintered in air at 1250 °C for 4 h with a heating rate of 3 °C min^{-1} and a cooling rate of 5 °C min^{-1}. After sintering, the resulting targets had a thickness of 3.5 mm. Their density was measured to be 97% of the theoretical value with the Archimedes' method and no porosity could be observed when looking at the cross-section of the pellets with scanning electron microscopy.

The LSCF dense layers (DL) were deposited with a PLD workstation from Surface GmbH (Hueckelhoven, Germany). The CGO pellets were placed in a substrate holder at a distance of 6 cm from the LSCF target. A base vacuum of 3 10^{-3} mTorr was established in the stainless steel chamber by means of a turbomolecular pump. The CGO substrates were heated up to 500 °C with a rate of 20 °C min^{-1}. Then the desired oxygen partial pressure (230 mTorr) was set by regulating the oxygen flow inside the vacuum chamber. This pressure was kept constant till the final venting of the vacuum chamber after deposition. From 500 to 800 °C, the substrate heating rate was 10 °C min^{-1}. Deposition was performed at 800 °C using a KrF (248 nm) excimer laser (ThinFilmStar V2.0, TuiLaser AG, Germany) with a nominal energy of 200 mJ per pulse, a repetition rate of 10 Hz and an incidence angle of 45 °C. The surface area of the laser beam impact on the target has been beforehand estimated to be 2 mm^2 by using

Table 2 Variation range of the adjustable parameters (***p***-components) in the NOP.

rds	500 °C	600 °C	Remarks/references
δ	10^{-4}–2 10^{-2}	10^{-4}–3 10^{-2}	
N (mol m^{-2})	10^{-3}–10^{-5}	10^{-3}–10^{-5}	
K_{ads} (mol^{-1} m^2 atm^{-1} s^{-1})	10^{-13}–10^{-4}	10^{-13}–10^{-4}	
K_{des} (mol^{-1} m^2 s^{-1})	10^{-13}–10^{-4}	10^{-13}–10^{-4}	
K_{out} (mol^{-3} m^9 s^{-1})	10^{-14}–10^{-10}	10^{-13}–10^{-9}	[13, 14]
D (m^2 s^{-1})	10^{-14}–10^{-10}	10^{-13}–10^{-9}	[13, 14]
k_{fb} (m s^{-1})	10^{-2}	10^{-2}	At quasi-equilibrium see results in Section 4

a YSZ pellet on which the ablated region is clearly visible. The effective laser fluence on the target that takes into account the optical losses of the beam line was ca. 8.5 J cm^{-2}.

During deposition, the target motion was a combination of rotation and translation to yield homogeneous ablation. The target rotation rate was 10 rpm and the translation velocity 16 mm s^{-1}. After deposition the substrate holder and the sample were cooled down till 140 °C with a rate of 10 °C min^{-1}, temperature at which the chamber was ventilated with argon. A growth rate of 175 nm h^{-1} has been evaluated for the deposition conditions described above. Typically a DL exhibits a columnar nanostructure with a mean column width of ca. 30 nm (Figs. 2 and 3). The LSCF films deposited by PLD were subsequently structured into 3×3 mm^2 square-shaped electrodes using photolithography.

3.3 Fabrication of the electrochemical cell

The collection of the current at the thin films has been done using a porous LSCF film (~30 μm after sintering) prepared by screen-printing. The LSCF powder (Praxair, 70 wt.%) was grinded together with a mixture of diethylene glycol monobutyl ether acetate (Fluka 32260, 24 wt.%), furan-2-carboxylic acid (Fluka 48000, 0.9 wt.%) and ethylcellulose (Fluka 46070, 5.1 wt.%) in a mortar till a homogeneous paste was obtained. The latter was screen-printed on top of the PLD-deposited film. A platinum mesh (Alfa Aesar, 52 mesh, 0.1 mm wire diameter, 99.9%) was slightly pressed on top of the screen-printed layer in order to ensure a good contact. A thin stripe (3 mm long, ~0.5 mm wide) of LSCF paste was painted 1 mm besides the working electrode and was used as reference electrode. A LSCF counter-electrode has been pasted on the opposite side of the CGO pellet symmetrically to the working electrode and contacted with a platinum mesh. The cell has been annealed in air at 800 °C during 2 h (heating and cooling rates 5 °C min^{-1}). A cross-section view of the LSCF/CGO interface is shown in Fig. 3.

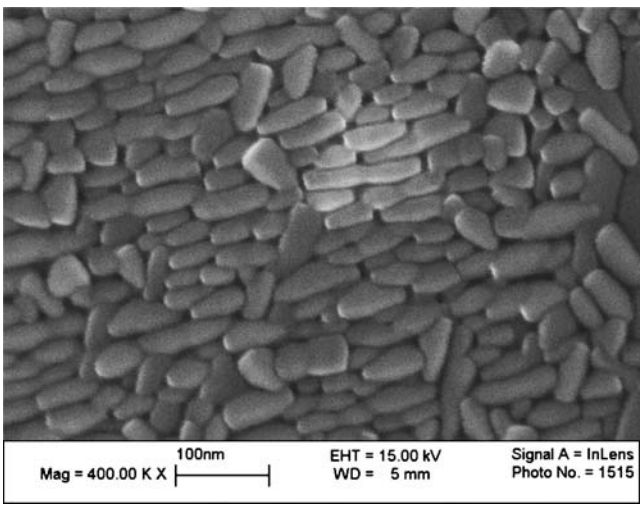

Fig. 2 Top-view micrograph of a LSCF layer prepared by pulsed laser deposition. The layer grew columnarly (see Fig. 3) with a mean column width of ca. 30 nm (after annealing at 800 °C)

One advantage of this type of current collection is to keep the platinum contact far away from the LSCF dense film as schematically described in Fig. 4.

In this work, it was assumed that gas phase diffusion is negligible and oxygen is incorporated in the DL (Fig. 4, pathway I) without significant contribution from the porous current collector (Fig. 4, pathway II). The effect of the platinum contact (Fig. 4, pathway III) was also ignored. Therefore the electrocatalytic properties measured during the study were believed to originate from the material of interest (LSCF) and not from the platinum. The role of the current collector is further discussed in Section 5. Porous LSCF electrodes without DL have been prepared following the same procedure by screen-printing the paste directly onto the CGO electrolyte.

3.4 Electrochemical experiments

A standard three electrodes cell driven by a potentiostat (Zahner IM-6) has been employed for the steady-state voltammetry and impedance experiments that were carried out in air at 500, 600 and 700 °C. The impedance of the LSCF/CGO interface was measured between 0.1 Hz and 100 kHz with 8 points per decade and ten periods for each

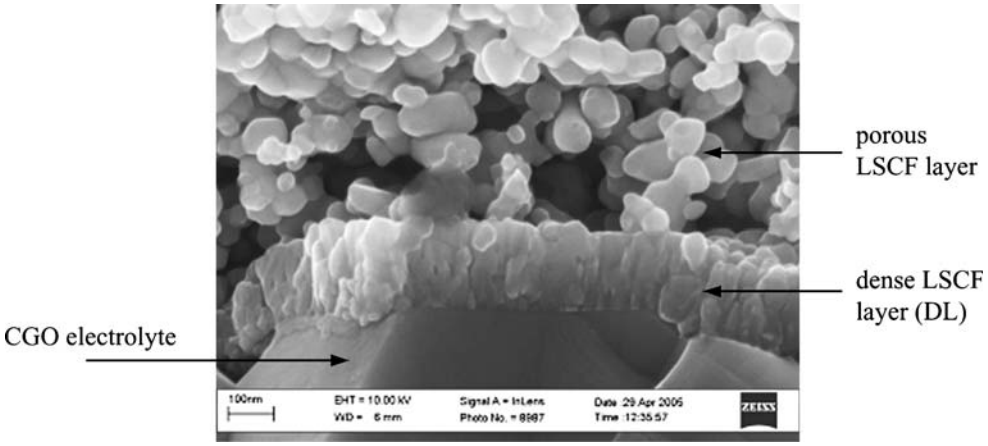

Fig. 3 Cross-section micrograph of a dense LSCF layer (*DL*) deposited by PLD on a polished CGO electrolyte. The DL exhibits a columnar structure with a typical column width of ca. 30 nm. The current collection is carried out by a porous LSCF layer

frequency using a 5 mV sinusoidal perturbation. The equilibrium potential of the oxygen reduction was 0 mV for each temperature.

4 Results

In what follows, all the impedances are expressed in Ω cm^2, if not otherwise mentioned. Oxygen reduction at the LSCF/CGO interface was investigated at 500, 600 and 700°C. The impedance of the reaction could be accurately measured only at 500 and 600 °C. At 700 °C the frequency response was too low (<0.1 Ω cm^2) and the faradaic and electrolyte impedances overlapped.

Typical as-recorded experimental impedance spectra (Z_{exp} expressed in ohms) are shown in Fig. 5. The high frequency impedance, Z_{high}, is quasi-independent of the electrode potential and is therefore attributed to the electrolyte (Z_e). The low frequency impedance, Z_{low}, corresponds to the electrochemical reaction. The capacitance, C_{low}, of Z_{low} can be estimated by approximating the frequency response in the complex plane as a semi-circle, i.e. a resistance R_{low} in parallel is C_{low}. Then

$$C_{low} = \frac{1}{R_{low} f_{low}} \tag{16}$$

with f_{low} being the relaxation frequency of Z_{low}.

C_{low} is found to range between 0.01 and 1 F cm^{-2} depending on the electrode potential and thickness. Typically C_{DL} values are two order magnitudes smaller (~10^{-4} F cm^{-2} for the $La_xSr_{1-x}Mn_yO_3$ (LSM)/yttria-stabilized zirconia interface [15]). C_{low} is therefore assigned to the faradaic impedance. C_{DL} can be neglected and $Z_F \sim Z_{low}$. Since Z_{exp} remains unchanged at high frequency when the electrode potential is varied and given that C_{DL} is negligible, it can be concluded that the charge transfer resistance R_1 is negligible, i.e. charge transfer at the electrode/electrode interface (rate constants K_{fb} and K_{bb}) is not rate-determining.

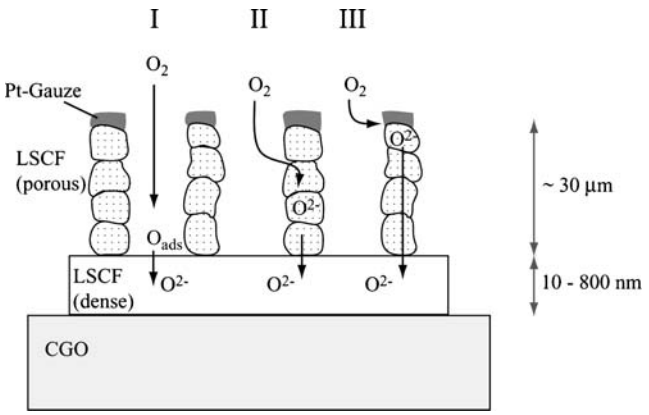

Fig. 4 Possible pathways for the access of molecular oxygen to the dense LSCF layer. Pathways II and III are assumed to be kinetically less favourable. The porous LSCF layer acts only as a current collector

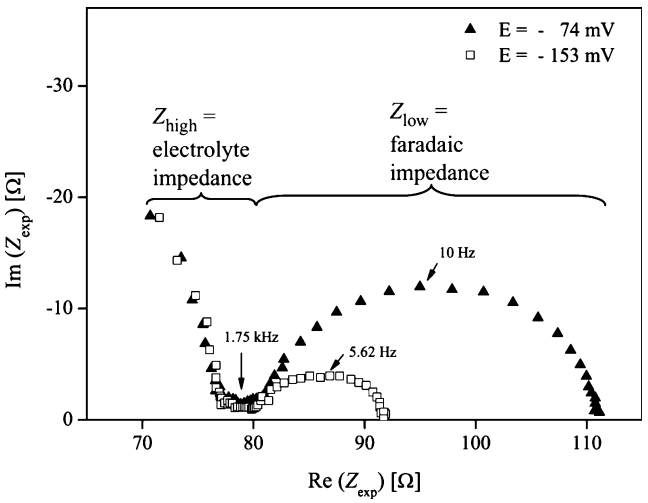

Fig. 5 Typical experimental Nyquist plots of oxygen reduction. The high frequency impedance Z_{high} that is quasi-independent of the applied potential is ascribed to the electrolyte (Z_e). The low frequency impedance Z_{low} corresponds to oxygen reduction

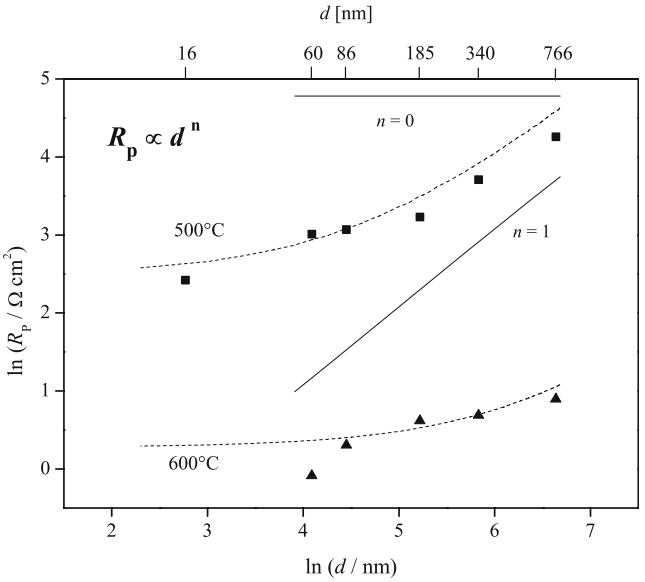

Fig. 6 Polarization R_p as a function of d at 500 and 600 °C at E= 0 mV. The full symbols (■, ▲) represent the experimental data. The dashed lines represent the simulated data from the model obtained after numerical optimisation (see rate constants in Table 3). Oxygen bulk diffusion appears to be one of the rds of the reaction

The influence of oxygen vacancy diffusion on the reaction kinetics has been investigated by measuring the polarisation resistance R_p as a function of d (Fig. 6). R_p increases with increasing d, which evidences that bulk diffusion is one of the rate-determining steps (*rds*). This is particularly true at 500 °C for the 340 and 766 nm samples. At this temperature, the quasi-linear dependence between R_p and d clearly shows that bulk diffusion is the dominant *rds*. The influence of diffusion decreases with decreasing thickness and increasing temperature. This indicates that at least one other reaction step is co-limiting the reaction kinetics. By extrapolation, it can be expected that, at 700°C, R_p is almost independent of d, i.e. the losses due to bulk diffusion are negligible.

At 600 °C, the 60 nm sample has a significantly lower polarization resistance and deviates from the model that is valid for thicker DL. This finding is confirmed by the DC behaviour of the thin films. Figure 7 shows the steady-state polarization curves for various temperatures. As expected, the activity of the electrodes increases with decreasing d and increasing temperature. At 600 °C, when d is reduced, the activity increases till it becomes quasi-independent of d (86–340 nm). When d is further reduced ($d \leq 60$ nm), the current density j is further enhanced. This points out a different reaction kinetics for ultrathin films.

This activity enhancement of the ultrathin films is even more pronounced at 700 °C where oxygen reduction exhibits very low overpotentials. The NOP enabled to assess the values of the rate constants and identify the rds

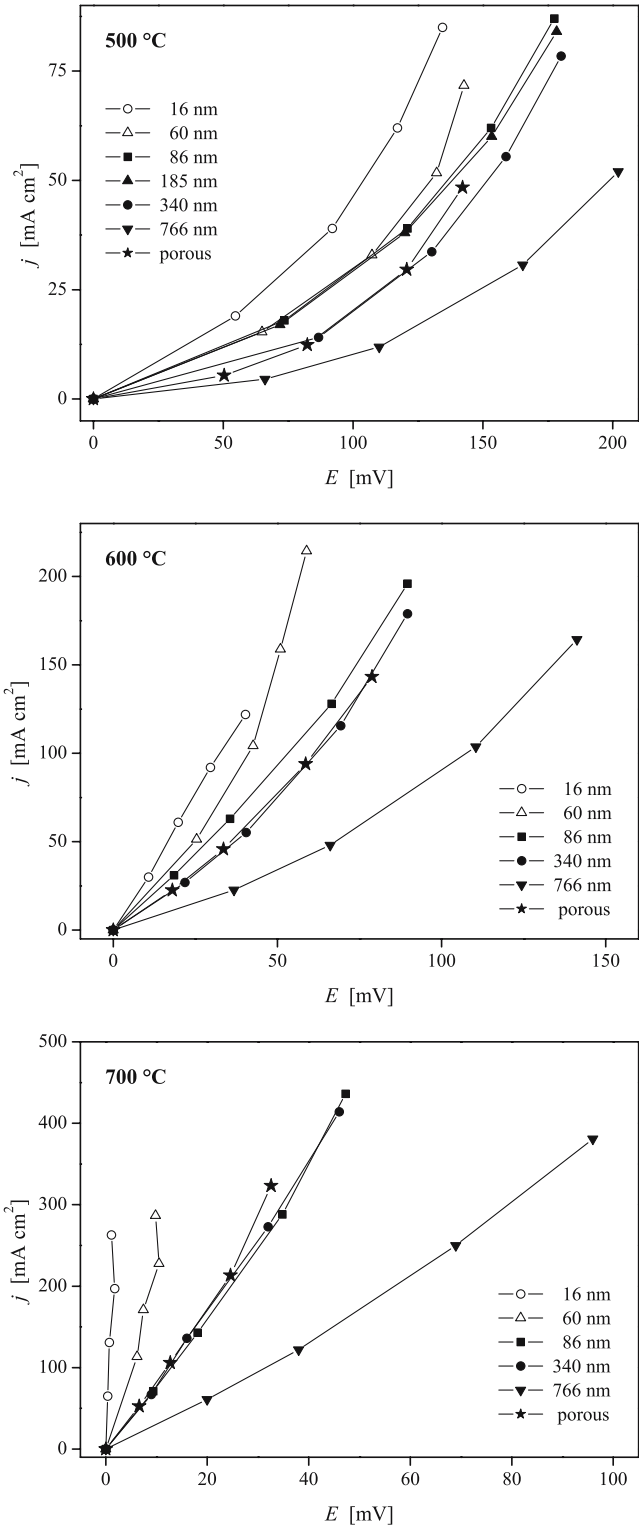

Fig. 7 Oxygen reduction polarization curves (ohmic drop corrected) of thin dense and thick porous LSCF electrodes at 500, 600 and 700°C in air. The best electrochemical performance is obtained with ultrathin dense electrodes

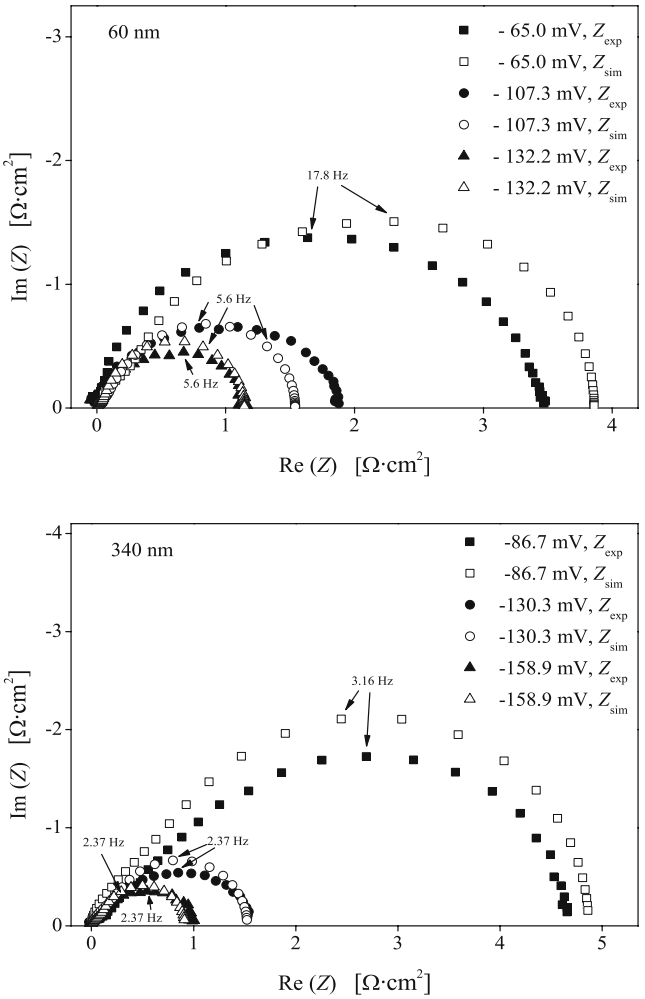

Fig. 8 Comparison of Z_{sim} and Z_{exp} at 500 °C (after removal of the electrolyte contribution) after the NOP. The acceptable agreement between both impedances makes possible the assessment of the kinetic parameters of the model (see Table 3). It reveals that oxygen adsorption and incorporation are rate-limiting together with bulk diffusion

of the reaction. Figure 8 shows typical results of the NOP and compares Z_{sim} and Z_{exp}. The simulated data describe reasonably well the experimental impedance and its variations with respect to the electrode potential and thickness. The resulting values of the kinetics parameters are listed in Table 3 and reveal that adsorption and incorporation are rate-determining. At 500 °C all the samples follow the same reaction kinetics. At 600 °C a separate NOP has been carried out for ultrathin films in order to clarify their peculiar behaviour. Their enhanced electroactivity is explained by slightly larger adsorption, incorporation and diffusion constants and significantly higher concentration of the oxygen vacancies (compared to thicker films), which promotes oxygen incorporation in the LSCF layer.

As demonstrated in [1], the use of thin dense electrodes does not enable to investigate the kinetics of the surface pathway of the reaction due to the too small tpb-length. However it is worth comparing the polarization curves of LSCF/CGO interfaces with and without thin dense film deposited by PLD. Figure 7 shows that, for a given potential, the current density of the porous electrodes is comparable to the one of thin films with intermediate thickness (86–340 nm). This finding suggests that the kinetics of the surface pathway of porous LSCF electrodes is not negligible. If the surface pathway was the only reaction pathway, the addition of the DL would markedly decrease the performance of the electrode by reducing the tpb-length to almost zero. In contrast, if the bulk pathway was the only reaction pathway, the addition of the DL would increase the performance of the electrode by enlarging the surface area of LSCF in contact with the electrolyte. The results shows that the best electrode performance is achieved by coating the electrolyte with an ultrathin DL that exhibits high electrocatalytic activity, large concentration of oxygen vacancies and almost no diffusion losses. However the benefits of these ultrathin DL are gradually lost when decreasing the temperature.

5 Discussion

The proposed reaction model describes reasonably well the oxygen reduction process at LSCF at intermediate temperatures. The reaction is kinetically limited by adsorption, incorporation and bulk diffusion steps while charge transfer is facile. These findings are in good agreement with the conclusions of Adler et al. [16] who investigated porous $La_{0.6}Ca_{0.4}Co_{0.2}Fe_{0.8}O_{3-\delta}$ and $La_{0.8}Sr_{0.2}CoO_{3-\delta}$ electrodes. The results on the comparison of interfaces with and

Table 3 Model parameters resulting from the NOP.

	500 °C	600 °C $d \geq 86$ nm	600°C $d=60$ nm[a]
K_{ads} ($mol^{-1}m^2\ atm^{-1}\ s^{-1}$)	10^7	$3.2\ 10^7$	$1.3\ 10^8$
K_{des} ($mol^{-1}\ m^2\ s^{-1}$)	10^5	10^6	10^6
K_{out} ($mol^{-3}\ m^9\ s^{-1}$)	10^{-12}	$8\ 10^{-12}$	$2\ 10^{-11}$
D ($m^2\ s^{-1}$)	$1.3\ 10^{-12}$	$1.6\ 10^{-11}$	$6.3\ 10^{-11}$
k_{fb} ($m\ s^{-1}$)	10^{-2} [b]	10^{-2} [b]	10^{-2} [b]
N ($mol\ m^{-2}$)	$4\ 10^{-5}$	$4\ 10^{-5}$	$4\ 10^{-5}$
δ	0.0004	0.002	0.011

[a] The 16 nm sample could not be analysed because the faradaic impedance could not be unambiguously discriminated from the electrolyte impedance.
[b] The fixed large value of k_{fb} reported in this table accounts for the fact that charge transfer remains at quasi-equilibrium.

without thin films suggest that the surface pathway contributes in a non-negligible manner to the overall process in the case of porous LSCF layers. The surface contribution could not be investigated with two-dimensional electrodes because of low tpb-length. Therefore the quantitative conclusions of this work cannot be transposed to conventional porous electrodes. As schematically illustrated in Fig. 9, oxygen reduction at thin dense films is one-dimensional with well-controlled bulk diffusion length. In the case of porous electrodes, the diffusion length is a priori unknown and depends on kinetics of both the surface and bulk pathways.

Table 4 compares the oxygen diffusivity, D_O, and oxygen exchange coefficient, k, obtained in this study (derived from Eqs. 13 and 15) with literature data that originate from $La_{0.6}Sr_{0.4}Co_{0.2}Fe_{0.8}O_{3-\delta}$ bulk samples measured with isotope exchange measurements. It appears that k is significantly higher in thin films than in bulk samples. D_O values are roughly of the same order of magnitude at 500 °C. At 600 °C the ultrathin films (d=60 nm) exhibit greater diffusivity. A tentative explanation is that k and D_O are influenced by the nanostructure of the DL. The PLD-deposited layers grow columnarly (Fig. 3) with a column width of ca. 30 nm. Thus the DL has many grain boundaries, which can modify the transport and catalyic properties compared to conventional SOFC materials with grains ranging typically between 100 nm and 1 μm. In recent years, ceramic nanomaterials and thin films have been drawing ever-growing interest [17], notably in fields such as of grain growth [18], electrical conductivity [19] micro-SOFC [20, 21] and geometrically well-defined electrodes [4–6]. Further work is still needed to clarify the effect of nanoscaled grain size on catalytic and transport properties of SOFC materials. This may help to develop innovating materials with new microstructures and design (thin dense rather than thick porous electrodes, for instance) for intermediate and low temperature fuel cell cathodes.

Combining state-space modelling and geometrically well-defined electrodes offer undeniable advantages for the investigation of SOFC processes, such as oxygen reduction. Nevertheless the use of thin mixed ionic–electronic conducting films presents also some drawbacks and raises new questions and problems.

Current collection is a crucial issue. When working with thick porous electrodes (typically >10 μm) prepared by conventional ceramic processing methods, this task is relatively straightforward. A metallic gauze (made of platinum, for instance) is pressed on the layer in its green state. Cofiring the paste and the current collector yields a good “intimacy” and reliable mechanical stability between both components. Homogeneous potential distribution is achieved throughout the bulk of highly conducting materials like LSCF and LSM. Current collection is more arduous when dealing with thin electrodes, such as PLD layers. Besides the fact that the films do not have any green state, two contradictory requirements have to be fulfilled. On one hand, molecular oxygen should have access to the thin layer, which implies a sufficient open porosity. On the other hand, in order to ensure a homogeneous potential distribution when working out of equilibrium, the current collector should have as many contact points as possible with the dense film that, in the ideal case, should be fully covered. In this work, the choice of a porous LSCF film as current collector is a compromise between these two constraints. However one has to keep in mind that the experimental system differs from the model (where a virtual collector has been used [1]) in the sense that the oxygen cannot adsorb uniformly all over the surface of the DL. The porous layer may also provide oxygen to the DL during the reduction process (see pathway II in Fig. 4) to a certain extent. More investigations have to be done to clarify this point and eventually refine the present reaction model.

Alternative current collection approaches could be considered in future studies, each of them having its own advantages and drawbacks. If the current collector is not of the same material than the DL, the kinetics of oxygen adsorption and incorporation cannot be exclusively assigned to LSCF, which is problematic for investigations of electrochemical properties of materials. A thin dense silver layer may be utilized since oxygen can diffuse through it. Ringuedé and Fouletier [22] employed this kind of current collector to investigate oxygen reduction at

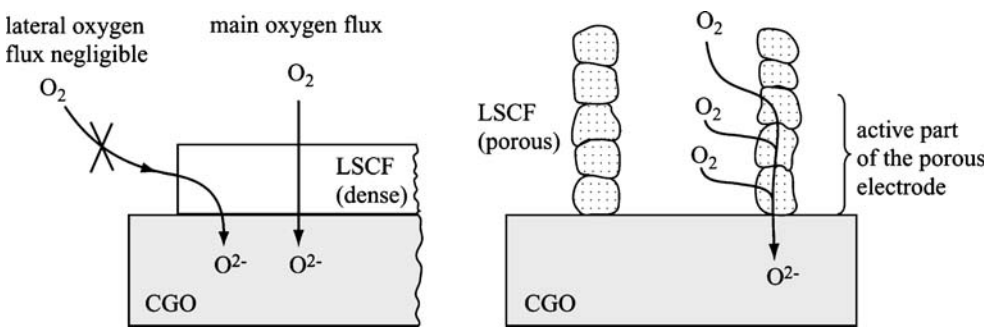

Fig. 9 Comparison of oxygen reduction pathways at thin dense (*left*) and thick porous (*right*) LSCF electrodes. Thin dense electrodes enable to control the bulk diffusion length of the one-dimensional oxygen reduction process

Table 4 Oxygen exchange coefficient and oxygen diffusivity of thin $La_{0.52}Sr_{0.48}Co_{0.18}Fe_{0.82}O_{3-\delta}$ films (evaluated in-situ at equilibrium) and bulk $La_{0.6}Sr_{0.4}Co_{0.2}Fe_{0.8}O_{3-\delta}$ samples (measured ex-situ with IEDP).

	500 °C this study	500 °C bulk sample IEDP [13, 14]	600 °C $d\geq$ 86 nm this study	600 °C d=60 nm this study	600 °C bulk sample IEDP [13, 14]
k (m s^{-1})	2.7 10^{-9}	~4 10^{-10}	3.3 10^{-8}	4.7 10^{-8}	10^{-9}–3 10^{-9}
D_O (m^2 s^{-1})	1.7 10^{-16}	6 10^{-16}–8 10^{-16}	1.1 10^{-14}	2.3 10^{-13}	~2 10^{-14}

$La_{0.7}Sr_{0.3}CoO_{3-\delta}$ electrodes. Porous LSM could be used since it exhibits sluggish oxygen transport properties and would provide only electrons to the DL. But the risk of contamination of the DL by the manganese is not to be excluded. Brichzin et al. [2] and Baumann et al. [23] collected the current by means of an external tungsten carbide tip when working with LSM and LSCF microelectrodes. It allows for a homogeneous access of oxygen to the gas/electrode interface. The contribution of the tip to the oxygen reduction can be neglected. Yet, when working with thin films, this kind of point contact may lead to heterogeneous potential and current distribution within the electrode.

Oxygen reduction at mixed ionic–electronic conductors is a particular type of electrochemistry since the bulk of the electrode directly participates to the reaction. In order to understand the oxygen reduction mechanism, it is therefore necessary to know the defect chemistry of LSCF at and out of equilibrium. It has been proven that the charge transfer step at the electrode/electrolyte is facile. This means that slow transport of oxygen may cause significant gradient of concentration in the bulk of the DL. Large depletion of oxygen can lead to the decomposition of the perovskite into the constituent oxides and modifications of the catalytic properties of the DL. In this study we have used a random defect model that ignores the interaction of oxygen vacancies (dilute solution approach) and cannot be applied at high oxygen deficiency. The electrochemical investigations have been restricted to relatively low current densities due to the choice of this defect chemistry model. Comprehending the behaviour of the LSCF perovskite at higher current densities requires answers to several questions that currently remain open. What is the maximum oxygen nonstoichiometry that the perovskite can withstand without undergoing decomposition? At high oxygen vacancy concentrations, what model can describe defect interactions? In the literature, defect chemistry models at low oxygen partial pressures involving clusters such as $\left\{B'_B - V''_O - B'_B\right\}^x$ [24, 25], $\left\{Sr'_{La} - V''_O\right\}^{\cdot}$ [26, 27] and, $\left\{B'_B - V''_O\right\}^{\cdot}$ [28] have been proposed for various perovskites at equilibrium. Can those models be applied when an ionic current flows through the mixed conductor? Elucidating those open questions constitute challenging and essential topics of future investigations.

In this work, for sake of simplicity and to keep the calculation costs of the numerical optimization process at a reasonable level, the flux of electronic species (and consequently ambipolar diffusion) in the bulk of the electrode has been neglected. Implementing it in the reaction mechanism would constitute a valuable refinement of the model. Even though this has no influence at low frequencies (the polarisation resistance remains unchanged), the faradaic impedance of oxygen reduction at $La_{0.52}Sr_{0.48}Co_{0.18}Fe_{0.82}O_{3-\delta}$ electrodes might be more affected at high frequencies. Jamnik et al. [29–31] investigated the coupling of ionic and electronic fluxes and derived a generalized equivalent circuit model. Unlike physical models, electrical equivalent circuits are not suitable for investigating reaction mechanisms and kinetics that are a priori unknown (like in the present study). However combining the general treatment of the fluxes of charged carriers (based on the Nernst–Planck equations) developed by Jamnik et al. with the thorough mechanistic description of the reaction model provided by the state-space modelling approach could lead to in-depth simulations of the oxygen reduction process.

6 Conclusions and outlook

Oxygen reduction at thin dense $La_{0.52}Sr_{0.48}Co_{0.18}Fe_{0.82}O_{3-\delta}$ films with well-controlled dimensions has been studied in air between 500 and 700 °C with steady-state voltammetry and impedance spectroscopy. Adsorption as well as oxygen incorporation and bulk diffusion in the LSCF govern the reaction kinetics while charge transfer remains at quasi-equilibrium. The use of geometrically well-defined electrodes combined with preliminary state-space modelling was of great help to identify the rate-determining steps of the reaction. Bulk diffusion has been evidenced by the increase of the polarization resistance upon increasing the film thickness. The rate constants have been assessed with a numerical optimisation process based on the reaction model.

Yet some theoretical and experimental aspects can be improved. Alternative current collection systems could be developed and tested in order to unambiguously understand its contribution to the electrochemical measurements. Defect chemistry of LSCF accounting for oxygen vacancy interactions at and out of equilibrium should be better

understood so that similar electrochemical investigations could be performed at high current densities. The influence of the electronic flux on the impedance at high frequency should be further studied. The results show that ultrathin films enhance the electrochemical performance of LSCF. Oxygen exchange coefficient and diffusion coefficient of thin films with nanosized grains differ from the ones of bulk materials. The comprehension of the relations existing between the nanostructure and the transport properties of materials would open new perspectives to tailor high performance SOFC cathodes for reduced temperature applications.

Acknowledgements The financial support of ETH-Zurich (project TH-6/00-2) is gratefully acknowledged. The authors thank L. Cavalli, S. Schlumpf and M. Koch for excellent technical support.

References

1. M. Prestat, J.F. Koenig, L.J. Gauckler, J. Electroceramics (in press, 2007)
2. V. Brichzin, J. Fleig, H.-U. Habermeier, J. Maier, Electrochem. Solid-state Lett. **3**, 403 (2000)
3. A. Bieberle, L.J. Gauckler, Solid State Ionics **146**, 23 (2002)
4. T. Horita, K. Yamaji, M. Ishikawa, N. Sakai, H. Yokokawa, T. Kawada, T. Kato, J. Electrochem. Soc. **145**, 3196 (1998)
5. T. Horita, K. Yamaji, N. Sakai, H. Yokokawa, T. Kawada, T. Kato, Solid State Ionics **127**, 55 (2000)
6. E. Koep, C. Compson, M. Liu, Z. Zhou, Solid State Ionics **176**, 1 (2005)
7. S. Wang, M. Katsuki, M. Dokiya, T. Hashimoto, Solid State Ionics **159**, 71 (2003)
8. D. Waller, J.A. Lane, J.A. Kilner, B.C.H. Steele, Solid State Ionics **86–88**, 767 (1996)
9. A.L. Shaula, V.V. Kharton, F.M.B. Marques, J. Eur. Ceram. Soc. **24**, 2631 (2004)
10. L.-W. Tai, M.M. Nasrallah, H.U. Anderson, D.M. Sparlin, S.R. Sehlin, Solid State Ionics **76**, 273 (1995)
11. R.J. Chater, S. Carter, J.A. Kilner, B.C.H. Steele, Solid State Ionics **53–56**, 859 (1992)
12. J.A. Kilner, R.A. De Souza, I.C. Fullarton, Solid State Ionics **86–88**, 703 (1996).
13. S.J. Benson, R.J. Chater, J.A. Kilner, in *Solid Oxide Fuel Cells V*, ed. by H. Yokokawa, S.C. Singhal (The Electrochemical Society, PV 1997-24, Pennington, NJ 1997), p. 596
14. B.C.H. Steele, J.M. Bae, Solid State Ionics **106**, 255 (1998)
15. M. Prestat, PhD thesis no. 16142, ETH-Zurich, Switzerland (2006)
16. S.B. Adler, J.A. Lane, B.C.H. Steele, J. Electrochem. Soc. **143**, 3554 (1996)
17. D. Beckel, A. Bieberle-Hütter, A. Harvey, A. Infortuna, U. Muecke, M. Prestat, J. L. M. Rupp, L. J. Gauckler, J. Power Sources, 2007 (submitted for publication)
18. J. Rupp, E. Jud, L.J. Gauckler, in *Proceedings of the 6th European Solid Oxide Fuel Cell Forum*, ed. By M. Mogensen (Lucerne, Switzerland, 2004), p. 1202
19. I. Kosacki, T. Suzuki, V. Petrovsky, H.U. Anderson, Solid State Ionics **136–137**, 1225 (2000)
20. D. Beckel, D. Briand, A. Bieberle-Hütter, J. Courbat, N. F. De Rooij, L. J. Gauckler, Power Sources, 2007 (in press)
21. D. Beckel, U. P. Muecke, T. Gyger, G. Florey, A. Infortuna, L. J. Gaukler, Solid State Ionics, 2007 (in press)
22. A. Ringuedé, .J. Fouletier, Solid State Ionics **139**, 167 (2001)
23. F. Baumann, J. Fleig, J. Maier, in *Proceedings of the 6th European Solid Oxide Fuel Cell Forum*, ed. By M. Mogensen (Lucerne, Switzerland, 2004), p. 1241
24. S. Diethlem, A. Closset, J. Van Herle, K. Nisancioglu, Electrochemistry **68**, 444 (2000)
25. V.L. Kozhevnikov, I.A. Leonidov, M.V. Patrakeev, E.B. Mitberg, K.R. Poeppelmeier, J. Solid State Chem. **158**, 320 (2001)
26. M.S. Islam, Solid State Ionics **154–155**, 75 (2002)
27. M.S. Cherry, M.S. Islam, C.R.A. Catlow, J. Solid State Chem. **118**, 125 (1995)
28. L. Gavrilova, V.A. Cherepanov, in *Solid Oxide Fuel Cells VI*, ed. By S.C. Singhal, M. Dokiya, (The Electrochemical Society Pennington, PV 1999-19, Pennington, NJ, 1999), p. 404
29. J. Jamnik, J. Maier, J. Electrochem. Soc. **146**, 4183 (1999)
30. J. Jamnik, J. Maier, S. Pejovnik, Electrochim. Acta **44**, 4139 (1999)
31. J. Jamnik, J. Maier, Phys. Chem. Chem. Phys. **3**, 1668 (2001)